



Dynamic water management of polymer electrolyte membrane fuel cells using intermittent RH control

I.S. Hussaini, C.Y. Wang*

Department of Mechanical and Nuclear Engineering, and Electrochemical Engine Center (ECEC), The Pennsylvania State University, University Park, PA 16802, USA

ARTICLE INFO

Article history:

Received 17 November 2009

Received in revised form

20 December 2009

Accepted 22 December 2009

Available online 14 January 2010

Keywords:

Polymer electrolyte fuel cell

Water management

Intermittent humidification

ABSTRACT

A novel method of water management of polymer electrolyte membrane (PEM) fuel cells using intermittent humidification is presented in this study. The goal is to maintain the membrane close to full humidification, while eliminating channel flooding. The entire cycle is divided into four stages: saturation and de-saturation of the gas diffusion layer followed by de-hydration and hydration of membrane. By controlling the duration of dry and humid flows, it is shown that the cell voltage can be maintained within a narrow band. The technique is applied on experimental test cells using both plain and hydrophobic materials for the gas diffusion layer and an improvement in performance as compared to steady humidification is demonstrated. Duration of dry and humid flows is determined experimentally for several operating conditions.

© 2010 Elsevier B.V. All rights reserved.

1. Introduction

Water management is one of the most challenging aspects of PEM fuel cell operation and has been the subject of numerous studies in fuel cell literature [1–4]. Its objective is to achieve the delicate balance between the two conflicting requirements: achieving membrane hydration and avoiding electrode flooding.

Hydration of the membrane is essential for minimizing its resistivity and hence the ohmic losses in the cell. External humidification is often used when reaction water is insufficient to achieve full hydration of the membrane, especially in the inlet regions. However, this leads to excess water build-up further down into the cell which causes flooding on the catalyst layer resulting in a reduction in active reaction area and hence a drop in performance. Moreover, the water eventually appears in gas channels leading to an increase in parasitic pumping power and even channel clogging. Thus, liquid water has a two-fold affect on system efficiency. A detailed experimental study documenting the impact of flooding on fuel cell performance was reported in [5].

Some success at controlling catalyst layer flooding is achieved by imparting hydrophobic properties to the gas diffusion layer (GDL) and by placing a highly hydrophobic micro-porous layer (MPL) between the catalyst layer and the GDL [1,6,7]. However, this technique does not address the problem in its totality as the water

eventually collects in the GDL and gas channels. In situ visualization studies using neutron radiography show evidence of liquid water on the cathode side [8–10]. Other attempts at water management range from studies with partial or no external humidification of reactants [11–13] to innovative methods such as using internal electro-osmotic pumps [14] and utilizing magnetic particles in the cathode catalyst layer [15]. While the absence of external humidification is certainly desirable, experimental studies by Buchi et al. [11] show a 20–40% loss in current density over prolonged period of operation. In recent years, interdigitated flow field has received increased attention as it addresses the problem of under-land flooding [4,16]. However, this is achieved at the expense of a reduction in overall system efficiency due to the higher pumping pressure needed for its operation. Therefore, in spite of numerous efforts, practical success at water management in fuel cells has so far been limited.

In this work, we present a novel method of water management suitable for fuel cells operating at constant current densities. The fundamental premise of this technique is that in order to achieve optimum performance from a fuel cell, excessive liquid water needs to be eliminated without affecting the water content in the membrane. To achieve this objective, a dynamic water management technique using intermittent external humidification is developed. By controlling the duration of humidified and dry streams, the water content in the membrane can be controlled, thus recovering ohmic overpotential. As a result, it is possible to achieve a better overall performance without sacrificing system efficiency. In the following sections, we present the details of the technique and a simplified mathematical analysis followed by experimental results.

* Corresponding author. Tel.: +1 814 863 4762; fax: +1 814 863 4848.
E-mail address: cxw31@psu.edu (C.Y. Wang).

Nomenclature

A	area (m^2)
C	concentration (kmol m^{-3})
D	diffusion coefficient ($\text{m}^2 \text{s}^{-1}$)
F	Faraday's constant ($96,487,000 \text{ C kmol}^{-1}$)
GDL	gas diffusion layer
h_m	mass transfer coefficient (m s^{-1})
HFR	high frequency resistance ($\text{m}\Omega \text{ cm}^2$)
i	current density (A cm^{-2})
i_0	exchange current density (A cm^{-2})
$J(s)$	Leverett function
k	permeability (m^2)
L	channel length
M	molecular weight (kg kmol^{-1})
n	number of electrons
N	number of moles (kmol)
p	pressure (kPa)
p_{sat}	saturation pressure (kPa)
RH	relative humidity
R_u	universal gas constant ($8.314 \text{ kJ kmol}^{-1} \text{ K}^{-1}$)
s	saturation
Sh	Sherwood number
t	time (s)
T	temperature (K)
u	velocity (m s^{-1})
V	voltage (V)

Greek symbols

α	net water transport coefficient
α_c	transfer coefficient on cathode
δ	thickness (m)
ε	porosity
η	overpotential (V)
λ	membrane water content
ρ	density (kg m^{-3})
σ	ionic conductivity of membrane phase
θ	contact angle
ζ	stoichiometry

Subscripts

a	anode
acl	anode catalyst layer
agdl	anode GDL
c	cathode
ccl	cathode catalyst layer
cgdl	cathode GDL
ch	channel
D	dry
f	final, flow
H	humid
i	initial
ion	ionomer
m	membrane
w	water

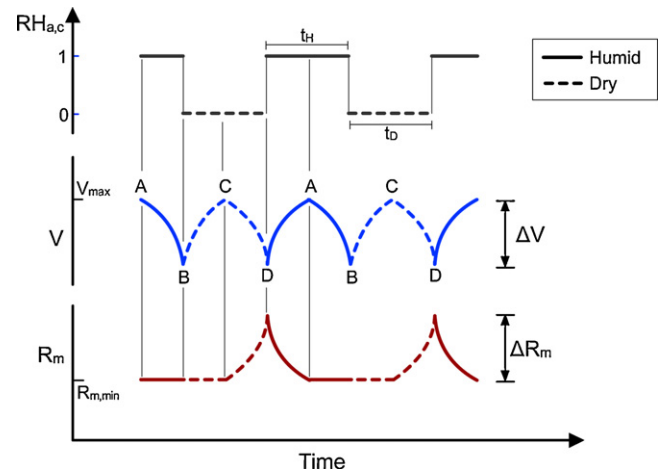


Fig. 1. Schematic diagram illustrating the technique of dynamic water management using intermittent humidification.

water coverage on catalyst layer (point A in Fig. 1). From this point onwards, the entire cyclic process can be considered to consist of four stages:

1. *Saturation of GDL (stage AB)*: Under humidified flow, product water is in liquid state and gradually covers up the catalyst layer surface causing a gradual drop in cell voltage. Humidified flow is continued until the voltage drops by a small amount ΔV . During this stage, the membrane is fully hydrated and its ionic resistance remains at the minimum.
2. *De-saturation of GDL (stage BC)*: During this stage, humidification is stopped and dry gases are passed into the cell. Water in the cell is picked up by the incoming dry gas streams causing a de-saturation of GDL and de-wetting of the CL. As a result, cell voltage recovers from B to C by the same amount ΔV . The membrane is unaffected during this stage and its resistance remains at the minimum.
3. *De-hydration of membrane (stage CD)*: Dry gas is continued during this stage which leads to onset of membrane de-hydration. Water diffuses out of the membrane and its ionic resistance increases causing the cell voltage to decline. Dry gas is allowed until the cell voltage decreases by ΔV .
4. *Hydration of membrane (stage DA)*: During this stage, external humidification is turned on. Hydration of membrane phase proceeds with the help of reaction water generated in the cell. Membrane resistance gradually decreases to its minimum value accompanied with a corresponding increase in cell voltage to point A, which represents the starting point in the cycle.

The humidified and dry cycles can thus be repeated in a cyclic manner to obtain sustained performance, with cell voltage always within a range of ΔV . With this technique, flooding on the cathode catalyst layer is contained and also, excess liquid water is prevented from accumulating in the GDL or gas channels thereby keeping the pressure drop to a minimum.

3. Mathematical analysis

In this section, a simple mathematical analysis for determining the duration of dry and humid flows is presented. The objective here is to identify the controlling phenomena and determine approximate time scales associated with each stage of the cycle.

2. Dynamic water management technique

The objective of this technique is to operate the fuel cell in the vicinity of its optimum performance by supplying humidified and dry inlet streams in a cyclic manner. Fig. 1 illustrates the details of the process. To begin with, consider the fuel cell at a state of maximum voltage under fully humidified reactant streams corresponding to a minimum membrane resistance and minimum liquid

3.1. Saturation of GDL

During this stage, product water is in liquid state which progressively builds up to cover the active reaction area. In order to maintain constant current, the uncovered surface operates at an elevated current density leading to higher activation overpotential and hence a corresponding drop in cell voltage.

The magnitude of liquid water coverage on the cathode catalyst layer ($S_{B,ccl}$) may be estimated by writing the Tafel equation at the initial and final states *A* and *B*. This is based on the assumption that cathode kinetics are sufficiently sluggish compared to the anode side [17]. Therefore, at a constant current density, we get

$$\eta_A = a + b \ln i \quad (1)$$

$$\eta_B = a + b \ln \left(\frac{i}{1 - S_{B,ccl}} \right) \quad (2)$$

where

$$a = \frac{R_u T}{\alpha_c n F} \ln i_0, \quad b = -\frac{R_u T}{\alpha_c n F}, \quad \eta_A - \eta_B = |\Delta V|$$

Combining the above equations, we get

$$S_{B,ccl} = 1 - \exp \left(-\frac{|\Delta V|}{b} \right) \quad (3)$$

At a temperature of 80 °C and with ΔV set at an arbitrary value of 10 mV, saturation on CCL at state *B* is obtained as 0.15. The corresponding saturation in cathode GDL is obtained by solving the capillary pressure continuity condition at the CCL and GDL interface (assuming no MPL) given below:

$$J(S_{B,cgdl}) = J(S_{B,ccl}) \frac{\cos \theta_{ccl}}{\cos \theta_{cgdl}} \sqrt{\frac{\varepsilon_{ccl} k_{cgdl}}{\varepsilon_{cgdl} k_{ccl}}} \quad (4)$$

For typical GDL properties [18], $S_{B,cgdl}$ from the above equation is about 0.10. An estimate of the time scale needed for this stage can then be obtained from the equation:

$$t_{AB} = \frac{\varepsilon_{cgdl} \delta_{cgdl} \rho_w S_{B,cgdl}}{(1 + 2\alpha) \cdot i / 2F \cdot M_w} \quad (5)$$

During this time, water accumulates on the anode side too, primarily by condensation. The resulting saturation in anode side GDL can be estimated from the equation

$$S_{B,agdl} = \frac{i}{2F} \left[\frac{p_{sat}(T)}{p - p_{sat}(T)} - 2\alpha \right] \frac{M_w}{\rho_w \delta_{agdl}} t_{AB} \quad (6)$$

However, it may be noted that the level of saturation on the anode side GDL is only a fraction of that in the cathode side GDL.

3.2. De-saturation of GDL

In this stage, dry reactants are used to evaporate the water accumulated in the anode and cathode GDL. However, there is a thermodynamic upper limit on the maximum amount of water vapor a stream can carry, which corresponds to an RH of 100%. Thus, in order for the reactant streams to dry the GDL, a necessary condition is that the amount of water carried out in the vapor phase is greater than the rate of water generation in the cell. With air on the cathode side and assuming equal anode and cathode stoichiometries, this requirement gives the condition

$$\frac{p_{sat}(T)/p}{1 - p_{sat}(T)/p} \left[(\zeta - 1) \frac{i}{2F} + (4.76\zeta - 1) \frac{i}{4F} \right] > \frac{i}{2F} \quad (7)$$

The expressions within the square brackets represent the water carried out in the vapor phase by the anode and cathode exhaust

streams respectively. On re-arranging, we get

$$\zeta > 0.29 \left(\frac{p}{p_{sat}(T)} - 1 \right) + 0.44 \quad (8)$$

At an operating temperature and pressure of 80 °C and 2 atm (abs) respectively, the minimum stoichiometry is calculated as 1.39. Therefore, only flow rates above this stoichiometry theoretically have the capacity to evaporate accumulated water. Below this stoichiometry, the liquid water generated in the cell continues to build up leading to flooding, even under completely dry flow. Under experimental conditions, this threshold may be slightly higher due to other factors such as design of flow field, effective mass transfer coefficient and so on.

The time scale for de-saturation of GDL is determined by considering the water removal rate at the channel exit. The governing equations for water conservation along anode and cathode channels, in counter-flow may be written as [19]:

$$\frac{\partial C_a}{\partial t} + u_a \frac{\partial C_a}{\partial x} + \frac{h_{m,a}}{\delta_{ch}} (C_a - C_{sat}) = 0 \quad (9)$$

$$\frac{\partial C_c}{\partial t} - u_c \frac{\partial C_c}{\partial x} + \frac{h_{m,c}}{\delta_{ch}} (C_c - C_{sat}) = 0 \quad (10)$$

with the initial and boundary conditions given by

$$C_a(x, 0) = C_{sat}, \quad C_c(x, 0) = C_{sat} \quad (11)$$

$$C_a(0, t) = 0, \quad C_c(L, t) = 0 \quad (12)$$

The mass transfer coefficients are obtained from the definition of Sherwood number as

$$h_m = Sh \frac{D_{w,cgdl}}{\delta_{ch}} \quad (13)$$

The value of Sherwood number is taken as 2.637 based on numerical results reported by Wang et al. [20]. Diffusion coefficients are estimated using Slattery–Bird correlation following the approach outlined by Springer et al. [21]. Solution to the above set of equations yields the concentration of water at the exit of the anode and cathode channels respectively. The time needed for this stage (t_{BC}) is then estimated from the following condition:

$$\int_0^{t_{BC}} \left(u_a A_f C_{w,a}(L, t) + u_c A_f C_{w,c}(0, t) - \frac{i A_m}{2F} \right) dt \geq \varepsilon_{gdl} \delta_{gdl} A_m \frac{\rho_w}{M_w} (S_{B,agdl} + S_{B,cgdl}) \quad (14)$$

3.3. De-hydration of membrane

During this stage, under continued dry gas flow, membrane and ionomers begin to lose water. Membrane water content across the catalyst layers and the membrane in the initial and final states is shown in Fig. 2. At state *C*, the membrane phase is hydrated whereas at *D*, it loses just enough water so that the ohmic loss is about $\Delta V/i$. The majority of this water is assumed to be removed from the anode side as this electrode does not generate water. The water content on the cathode side, however, may be assumed to remain unchanged during this interval. Moreover, if the water content in the membrane is assumed to vary linearly and its variation across the catalyst layers is neglected, then the total amount of water (in kmol) to be removed from the membrane phase, shown as the hatched region in Fig. 2, can be approximated as

$$N_{w,CD} = \frac{\rho_m A_m}{M_m} \left(\varepsilon_{ion} \delta_{acl} + \frac{\delta_m}{2} \right) (\lambda_{a,i} - \lambda_{a,f}) \quad (15)$$

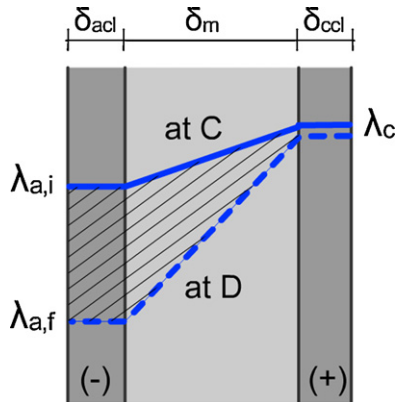


Fig. 2. Initial and final membrane water content as assumed in this analysis.

where $\lambda_{a,f}$ is obtained from the condition

$$\Delta R_{m,acl} + \Delta R_m = \frac{\Delta V}{i} \quad (16)$$

In the above equation,

$$\Delta R_{m,acl} = \frac{\delta_{acl}}{\varepsilon_{ion} \tau} \left(\frac{1}{\sigma(\lambda_{a,f})} - \frac{1}{\sigma(\lambda_{a,i})} \right) \quad (17)$$

$$\Delta R_m = \int_{\lambda_{a,f}}^{\lambda_c} \frac{dy}{\sigma(\lambda)} - \int_{\lambda_{a,i}}^{\lambda_c} \frac{dy}{\sigma(\lambda)} \quad (18)$$

The water content in the membrane at state C is determined using the one-dimensional model of Springer et al. [21]. The duration of dry gas flow t_{CD} during this stage is then determined from the condition:

$$\int_0^{t_{CD}} \left(u_a A_f C_{w,a}(L, t) + u_c A_f C_{w,c}(0, t) - \frac{i A_m}{2F} \right) dt \geq N_{w,CD} \quad (19)$$

3.4. Hydration of membrane

During this stage, external humidification is turned on. Water in the membrane is replenished primarily with reaction water and the time scale for the membrane to re-hydrate may be estimated from the equation [18]:

$$t_{DA} \approx N_{w,CD} \left(\frac{i A_m}{2F} \right)^{-1} \quad (20)$$

Table 1
Typical time scales for the duration of humidified and dry flows.

Current density (A cm ⁻²)	$\delta_m = 30 \mu\text{m}$		$\delta_m = 30 \mu\text{m}$		$\delta_m = 128 \mu\text{m}$	
	$\zeta = 2$		$\zeta = 4$		$\zeta = 4$	
	t_H (s)	t_D (s)	t_H (s)	t_D (s)	t_H (s)	t_D (s)
0.2	68	168	65	51	94	65
0.5	23	56	22	16	27	21
0.8	13	32	13	10	15	12

Therefore, the total duration of dry and humid flows for cyclic operation are

$$t_H = t_{AB} + t_{DA} \quad (21)$$

$$t_D = t_{BC} + t_{CD} \quad (22)$$

Table 1 gives a summary of the estimated time scales as a function of current density for two representative stoichiometries of 2 and 4, and membrane thicknesses of 30 μm and 128 μm . Flow field geometry corresponds to the 5 cm² test cell described in the following section. Plain, untreated GDL is assumed in this analysis, with dry and humidified flow at 0 and 100% RH respectively. The duration of humid flow is governed by the operating current density whereas the duration of dry gas flow is found to be strongly dependent on stoichiometry.

It is seen that the duration of dry/humid flows becomes progressively smaller as current density increases which is due to high flow rates at these conditions. The high current density region represents a drier membrane and thus offers a greater potential to recover ohmic losses. The effect of membrane thickness on flow duration is also observed from the data in Table 1. Thicker membranes hold more water and hence the time needed for their hydration and de-hydration is longer.

4. Experimental

4.1. Test cells

This technique is demonstrated in two test cells with different flow fields. A schematic of the flow fields in the two cells is shown in Fig. 3. The first is of 5 cm² effective area with a 13-turn, single channel serpentine flow field of dimensions 1 mm \times 0.75 mm \times 30 cm. The MEA used in this cell consists of a 30 μm GoreTM membrane and catalyst layers with 0.4 mg cm⁻² Pt-loading on each side. A plain, untreated Toray-060 carbon paper is used as the GDL.

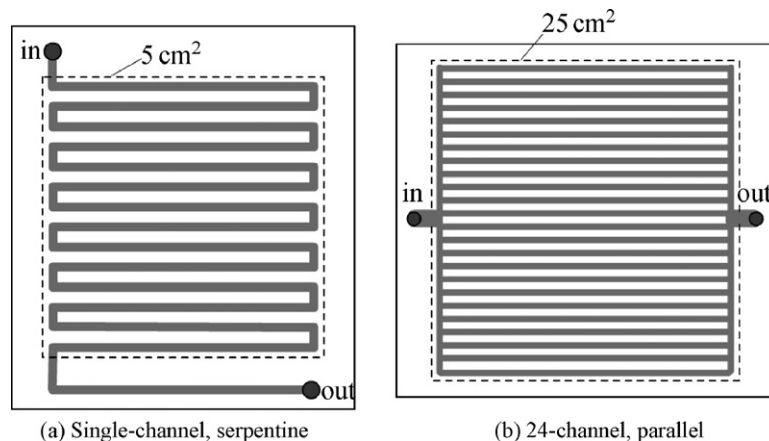


Fig. 3. Schematic of the flow fields in the two test cells considered in this study.

The other cell is of 25 cm² area with a 24-channel parallel flow field with each channel being 1 mm × 0.75 mm × 5.2 cm. The GDL used in this cell is a Toray-060 carbon paper coated with MPL and treated with Teflon for hydrophobicity. The MEA is of the same configuration as the 5 cm² cell. A straight-channel flow field is one of the simplest to manufacture and requires minimum overhead in terms of pumping pressure. However, such a configuration is also known to be prone to channel flooding even at low humidification [5].

4.2. Test setup and instrumentation

Experiments are conducted on a Teledyne™ fuel cell test station capable of controlling reactant flow rates and humidification levels, along with a data acquisition system for measuring cell voltage and membrane HFR in real-time through a PC-based software. The sampling interval for voltage and HFR are set at 1 and 2 s respectively. Humid or dry flow is controlled with the help of valves provided on the machine. High purity hydrogen is used on the anode and breathing air is used on the cathode.

4.3. Operating conditions and test procedure

The cells are operated at a temperature of 80 °C measured in the interior of the graphite bi-polar plate and at a back pressure of 2 atm (abs). The reactants are at 0 and 100% humidification during the dry and humid phases respectively. Flow stoichiometries of 3 and 4 and current densities of up to 1 A cm⁻² are investigated in this study. The test protocol is as follows:

1. The cell is initially purged of liquid water by passing dry inert gases at flow rates corresponding to a stoichiometry of 10 at 1 A cm⁻² for a period of 10 min.
2. Thereafter, dry reactants are passed for another period of 2 min at open circuit. Then, the flow rate is set to the required stoichiometry and open-circuit operation continued for a further 2 min. This process eliminates any residual water from previous test runs.
3. External humidification is turned on and a constant current density is set. Voltage and HFR are monitored in real time. Initially, the cell voltage is low due to high membrane HFR (a consequence of purging) and gradually increases with membrane hydration until it reaches a peak which corresponds to point A in Fig. 1. Thereafter, as catalyst layer flooding sets in, cell voltage begins to decrease.
4. After allowing the voltage to drop by about 10 mV (point B), humidification is turned off. Thereafter, under dry gas flow, the voltage peaks and then decreases again corresponding to points C and D.
5. The process is repeated and after a few cycles, the voltage and HFR reach a stable pattern. The mean duration of dry and humidified flows is then determined. The average value of cell voltage and HFR are also calculated for comparison with the results from steady humidification.

5. Results and discussion

5.1. Single-channel, serpentine flow field

Results are first presented for the 5 cm² cell with a single-channel serpentine flow field installed with a plain, untreated GDL. In the absence of MPL and hydrophobic treatment, the GDL material tends to hold more liquid water and thus the performance is generally low under steady state humidification. However, with the

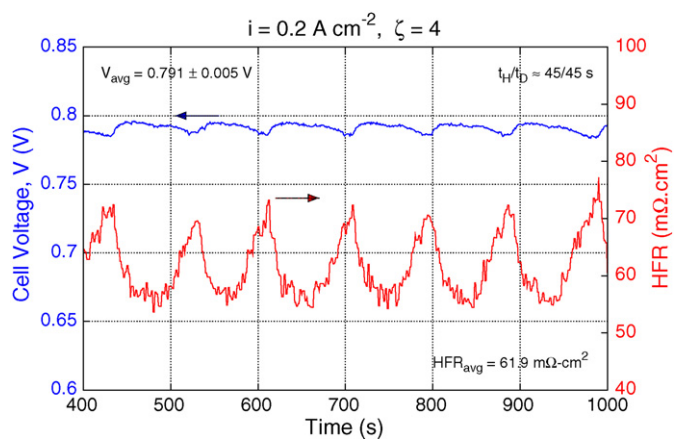


Fig. 4. Operation of the 5 cm² cell using intermittent humidification.

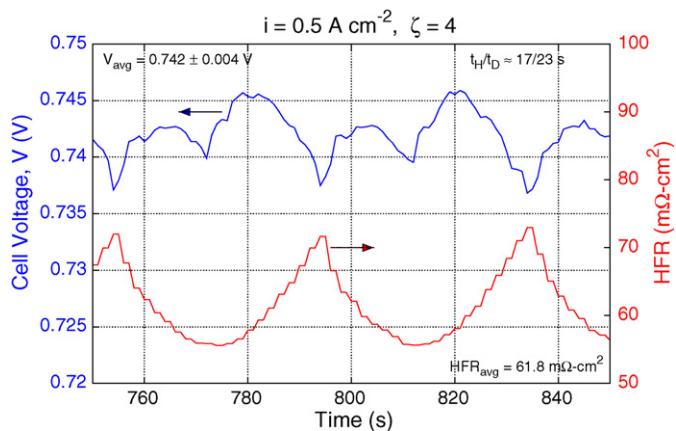


Fig. 5. Voltage and HFR response at a current density of 0.5 A cm⁻² and a stoichiometry of 4, shown on a magnified scale.

intermittent humidification technique, the level of liquid water in the cell can be minimized thus extracting better performance from the cell.

Fig. 4 shows the fuel cell operation with intermittent humidification at a current density of 0.2 A cm⁻² and a stoichiometry of 4. The points A, B, C and D correspond to the stages discussed earlier with reference to Fig. 1. Stable and sustained operation for a period of 10 min is shown in this figure. The voltage is maintained within a range of ±10 mV for the entire duration demonstrating consistency of the technique.

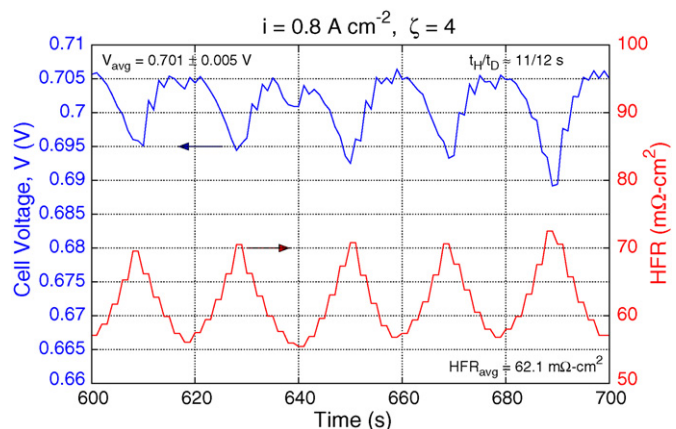


Fig. 6. Voltage and HFR response at a current density of 0.8 A cm⁻² and a stoichiometry of 4.

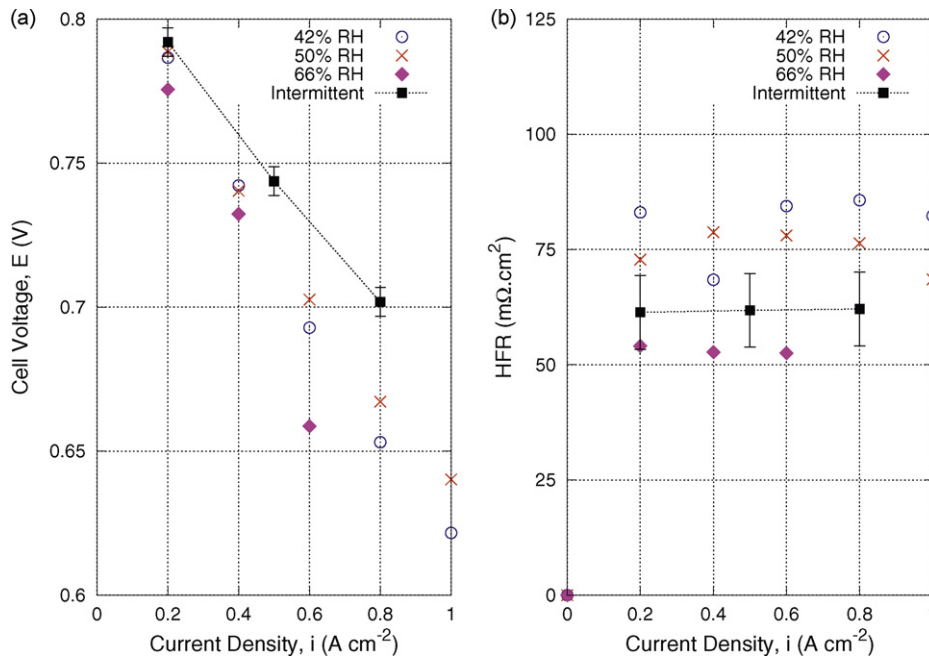


Fig. 7. Comparison of voltage and membrane HFR with steady and intermittent humidification (all data at a flow stoichiometry of 4).

Fig. 5 shows the voltage and HFR variation with time at current density and stoichiometry of 0.5 A cm^{-2} and 4 respectively. The various stages are clearly distinguishable in this figure. The duration of dry and humid flows is found to be generally in the range given in Table 1.

Fig. 6 shows the voltage and HFR response at an operating condition corresponding to 0.8 A cm^{-2} and a stoichiometry of 4. The duration of stages AB and BC are not clearly distinguishable which is due to the fact that at this current density and stoichiometry, these stages occur in very short times. Also, as anticipated from Table 1, the duration of dry and humid flows is lower at higher current densities.

A comparison of cell voltage and membrane HFR from polarization data under steady humidification and with intermittent humidification are shown in Fig. 7(a) and (b) respectively. Error bars on the data points for intermittent humidification represent the range within which the values lie during the dry and humid cycles. Values under steady humidification refer to the average value over 5 min after a 10-min period of operation at each condition. Humidification levels of 42, 50 and 66% RH are considered in this study. The results clearly demonstrate improved cell performance with intermittent humidification. The improvement in cell voltage is found to be about 8, 20 and 32 mV at 0.2 , 0.5 and 0.8 A cm^{-2} respectively. It is calculated as the difference between average cell voltage with intermittent humidification and the best voltage achieved with steady humidification among the various levels considered. It is noted that a substantial recovery in cell voltage is made possible by using this technique.

Fig. 7(b) illustrates the effectiveness of the intermittent humidification technique in keeping the membrane in a well-hydrated condition as evident from the low membrane HFR values. A well-hydrated membrane leads to lower ohmic losses in the membrane phase and a drier channel leads to lower energy losses in flowing the reactants, both of which contribute to a better cell performance and overall system efficiency.

Table 2 gives a comparison of test results at stoichiometries of 3 and 4. The duration of dry and humidified flows and the resulting average cell voltage and membrane HFR are also shown.

5.2. Multiple-channel, parallel flow field

Results are now presented for the 25 cm^2 cell shown in Fig. 3b. With a channel velocity being about 5-times lower than that in the serpentine-channel flow field, this configuration is more prone to channel flooding at low current densities and stoichiometries. Following paragraphs give the results obtained by operating the cell using intermittent humidification at various current densities. Dry and fully humidified air are used during the dry and humid operations respectively.

Fig. 8 shows a plot of voltage and membrane HFR with time for this cell at a current density of 0.8 A cm^{-2} and stoichiometry of 3. Stable operation for over 10 min is shown in this figure which demonstrates the ability to sustain the average voltage over several cycles of operation. It is observed that the GDL-saturation and de-saturation stages (AB and BC) and membrane hydration and de-hydration stages (DA and CD) are non-symmetrical which

Table 2
Summary of test results for the single-channel serpentine flow field fitted with untreated, plain GDL.

Stoichiometry ζ	Current density (A cm^{-2}) i	Time intervals (s) t_H/t_D	Voltage (V) $V_{\text{avg}} \pm \Delta V/2$	Membrane HFR ($\text{m}\Omega \text{ cm}^2$) $\text{HFR}_{\text{avg}} \pm \Delta \text{HFR}/2$
3	0.2	55/100	0.760 ± 0.005	57.5 ± 8
	0.5	10/20	0.721 ± 0.005	76.7 ± 14
	0.8	12/22	0.684 ± 0.015	67.5 ± 12
4	0.2	45/45	0.792 ± 0.005	61.4 ± 8
	0.5	17/23	0.742 ± 0.004	61.8 ± 7
	0.8	11/12	0.701 ± 0.005	62.1 ± 8

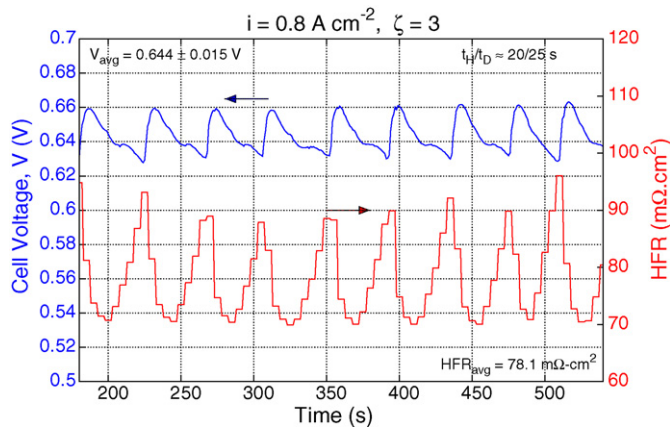


Fig. 8. Variation of cell voltage and membrane HFR with time at 0.8 A cm^{-2} and a stoichiometry of 3.

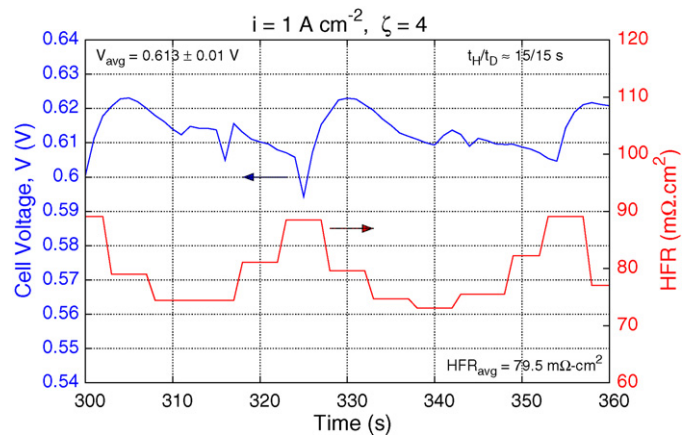


Fig. 10. Voltage and membrane HFR at 1 A cm^{-2} and at a stoichiometry of 4.

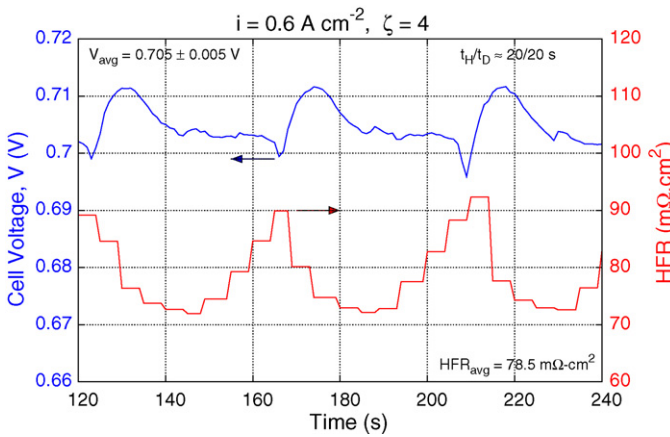


Fig. 9. Voltage and membrane HFR at 0.6 A cm^{-2} and at a stoichiometry of 4.

indicates that there are multi-dimensional effects which come into play and influence the variation of overall cell voltage and membrane HFR with time. It is also observed that the average membrane HFR is higher than that for the serpentine-channel flow field. This is apparently due to a higher contact resistance in this cell.

Figs. 9 and 10 show the variation of cell voltage and membrane HFR with time at current densities of 0.6 and 1 A cm^{-2} respectively, and at a flow stoichiometry of 4. Average membrane HFR is maintained at a low value indicating that ohmic losses in the membrane phase are minimized.

Similar tests are carried out over a range of current densities. Fig. 11 shows a comparison of average cell voltage and membrane HFR under intermittent and steady external humidification. Error bars represent the variation in the parameter over the entire cycle. For the range of current densities considered, an improvement in cell performance to the extent of 27 mV at 1 A cm^{-2} is achieved. The gain in voltage is higher at higher current densities. This is due to the fact that at high currents, ohmic losses are relatively higher.

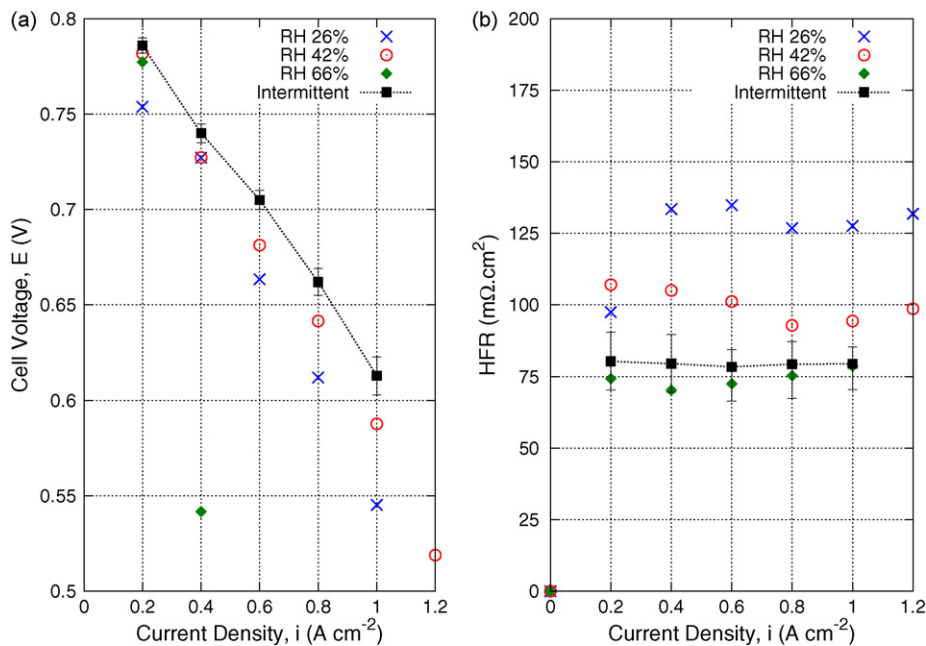


Fig. 11. Comparison of cell voltage and membrane HFR under steady and intermittent humidification, at a stoichiometry of 4.

Table 3

Summary of test results for the multiple-channel parallel flow field with a hydrophobic GDL coated with MPL. All data correspond to a stoichiometry of 4.

Current density ($A\text{ cm}^{-2}$) <i>i</i>	Time intervals (s) t_H/t_D	Voltage (V) $V_{avg} \pm \Delta V/2$	Membrane HFR ($m\Omega\text{ cm}^2$) $HFR_{avg} \pm \Delta HFR/2$
0.2	50/30	0.786 ± 0.004	80.4 ± 10
0.4	35/20	0.740 ± 0.005	79.6 ± 10
0.6	20/20	0.705 ± 0.005	78.5 ± 10
0.8	20/20	0.662 ± 0.007	79.4 ± 10
1.0	15/15	0.613 ± 0.010	79.5 ± 10

Therefore, the margin for voltage gain in such cases is comparatively higher. Table 3 gives a summary of the duration of dry and humid intervals and the resulting cell voltage and membrane HFR at various current densities.

Tests could not be carried out at current densities greater than 1 A cm^{-2} with sufficient repeatability primarily due to the fact that the duration of dry and humid flows at these conditions is of the order of 5 seconds. At such intervals, maintaining precise timing of dry and humid flows using a manual switching method was found to be difficult.

On the basis of this experimental study, it is seen that by providing intermittent humidification, a well-hydrated membrane and absence of flooding can be achieved. Voltage gain of the order of 30 mV, as compared to operation under steady humidification, has been demonstrated on two experimental-scale test cells.

6. Conclusions

Following are the main conclusions from this study:

1. A dynamic technique for water management in PEM fuel cells using intermittent external humidification has been presented. The technique involves cycling humidified and dry gases in the fuel cell at regulated time intervals with the objective of eliminating channel flooding and simultaneously maintaining a hydrated membrane.
2. The various stages of the cyclic process have been identified and an estimate of relevant time scale of each process has been presented.
3. The duration of humid cycle is found to be primarily a function of operating current density whereas the duration of the dry cycle shows a strong dependence on flow stoichiometry.
4. The technique has been demonstrated on an experimental test cell with a single-channel serpentine flow field fitted with a plain, untreated GDL as well as on a cell with a multiple, parallel-channel flow field, fitted with a hydrophobic GDL coated with MPL.

5. Improvement in performance up to 30 mV at 0.8 A cm^{-2} , as compared to the cell voltage with steady humidification, is obtained. The gain in voltage is higher at higher current densities due to recovery of ohmic losses in the membrane.

Acknowledgements

Partial support of this work by Ford Motor Co. through a University Research Program is gratefully acknowledged. I.S.H. also acknowledges King Abdullah University of Science and Technology (KAUST), Saudi Arabia for a fellowship award.

References

- [1] C.Y. Wang, Chem. Rev. 104 (10) (2004) 4727–4766.
- [2] T.F. Fuller, J. Newman, J. Electrochem. Soc. 140 (5) (1993) 1218–1225.
- [3] P. Berg, K. Promislow, J. Pierre, J. Stumper, B. Wetton, J. Electrochem. Soc. 151 (2004) A341.
- [4] T. Van Nguyen, M. Knobbe, J. Power Sources 114 (1) (2003) 70–79.
- [5] I.S. Hussaini, C.Y. Wang, J. Power Sources 187 (2) (2009) 444–451.
- [6] U. Pasaogullari, C.Y. Wang, Electrochim. Acta 49 (25) (2004) 4359–4369.
- [7] C. Lim, C. Wang, Electrochim. Acta 49 (24) (2004) 4149–4156.
- [8] R.J. Bellows, M.Y. Kin, M. Arif, A.K. Thompson, D. Jacobson, J. Electrochem. Soc. 146 (3) (1999) 1099–1103.
- [9] D. Kramer, J. Zhang, R. Shimoi, E. Lehmann, A. Wokaun, K. Shinohara, G.G. Scherer, Electrochim. Acta 50 (13) (2005) 2603–2614.
- [10] M.A. Hickner, N.P. Siegel, J.S. Chen, D.N. McBrayer, D.S. Hussey, D.L. Jacobson, M. Arif, J. Electrochem. Soc. 153 (5) (2006) A902–A908.
- [11] F.N. Buchi, S. Srinivasan, J. Electrochem. Soc. 144 (8) (1997) 2767–2772.
- [12] H. Yu, C. Ziegler, J. Electrochem. Soc. 153 (3) (2006) A570–A575.
- [13] J.R. Atkins, S.C. Savett, S.E. Creager, J. Power Sources 128 (2) (2004) 201–207.
- [14] C.R. Buie, J.D. Posner, T. Fabian, S.-W. Cha, D. Kim, F.B. Prinz, J.K. Eaton, J.G. Santiago, J. Power Sources 161 (1) (2006) 191–202.
- [15] L. Wang, N. Wakayama, T. Okada, Electrochem. Commun. 4 (7) (2002) 584–588.
- [16] Z.H. Wang, C.Y. Wang, Proceedings of the ASME Heat Transfer Division, American Society of Mechanical Engineers, 2000, p. 27.
- [17] U. Pasaogullari, C.Y. Wang, J. Electrochem. Soc. 151 (3) (2004) A399–A406.
- [18] Y. Wang, C.Y. Wang, Electrochim. Acta 50 (6) (2005) 1307–1315.
- [19] P. Sinha, C. Wang, J. Electrochem. Soc. 154 (2007) B1158–B1166.
- [20] Z.H. Wang, C.Y. Wang, K.S. Chen, J. Power Sources 94 (1) (2001) 40–50.
- [21] T.E. Springer, A. Zawodzinski, S. Gottesfeld, J. Electrochem. Soc. 138 (8) (1991) 2334–2342.